SI1. OPs and Structural Characterization of Macromolecular Systems

A simple case of the $\vec{R}^S, \vec{\Phi}_k$ relationship suggests how it captures rigid rotation. Take $U_k, k = 100, 010, 001$ to be X^0, Y^0 and Z^0 respectively. Then neglecting the residuals, Eq. (II.4) becomes $X_i = \Phi_{100\mathrm{X}} X_i^0 + \Phi_{010\mathrm{Y}} Y_i^0 + \Phi_{001\mathrm{Z}} Z_i^0$, and similar for Y_i and Z_i (where X_i, Y_i, Z_i are the three Cartesian components of $\vec{R}^S$ vector and $\Phi_{\underline{k}\alpha}$ is the α^{th} component of $\vec{\Phi}_k$). The relationship can be written in the tensorial form $\vec{R}^S = \bar{\bar{\Phi}}\, \vec{R}^{S,0}$. It is seen that for a special case (i.e., where the tensor $\bar{\bar{\Phi}}$ is a rotation matrix), $\vec{\Phi}_{\underline{k}}$ constitute a length preserving rotation about the assembly CM if $\vec{R}^S$ for the S^{th} subsystem is measured relative to this CM. More generally, for the above three basis functions, the $\vec{R}^S, \vec{\Phi}_k$ relationship corresponds to a mixed rotation, extension/compression. In fact the OPs defined here constitute a strain tensor thereby accounting for elastic deformations.

Transformations captured via these OPs are further understood below in terms a set of fundamental global and local deformations [30]. Consider the example of a tapering deformation (Fig. SI1). Take $U_k, k = 100, 110, 101$ to be X^0, X^0Y^0 and X^0Z^0 respectively. Again, neglecting residuals, Eq. (II.4) becomes $X_i = \Phi_{100\mathrm{X}} X_i^0 + \Phi_{110\mathrm{X}} X_i^0 Y_i^0 + \Phi_{101\mathrm{X}} X_i^0 Z_i^0$, and similarly for Y_i and Z_i. This relationship can be written in the tensorial form

$$\begin{pmatrix} X_i \\ Y_i \\ Z_i \end{pmatrix} = J \begin{pmatrix} X_i^0 \\ Y_i^0 \\ Z_i^0 \end{pmatrix}; J = \begin{pmatrix} \Phi_{100\mathrm{X}} & \Phi_{110\mathrm{X}} & \Phi_{101\mathrm{X}} \\ \Phi_{100\mathrm{Y}} & \Phi_{110\mathrm{Y}} & \Phi_{101\mathrm{Y}} \\ \Phi_{100\mathrm{Z}} & \Phi_{110\mathrm{Z}} & \Phi_{101\mathrm{Z}} \end{pmatrix}. \qquad \textbf{(S1.1)}$$

When $\Phi_{100x}, \Phi_{100y}, \Phi_{110x}, \Phi_{110z} = 0$ and $\Phi_{100x}, \Phi_{110y}, \Phi_{101z}, \Phi_{101y}, \Phi_{101x} \neq 0$, J is the Jacobian matrix for tapering along the X-axis [30]. Thus, these OPs capture structures that are tapered with respect to the reference configuration. Similar matrices can be constructed using other combinations of OPs to explain the twisting and bending transitions of Fig. SI1. Thus, the space warping variables characterize overall structure of an assembly. For relatively simple structural transitions, such as those of Fig. SI1, deformations of the assembly are defined via changing OPs for long periods of time with respect to a fixed reference configuration of subsystem CMs. However, to capture more complex structural transitions as described in Sect. V, the OPs as well as the reference configuration are allowed to evolve in time; the reference configuration though changes slower than the OPs. Thus, within a time window when change in the U_k is negligible, but the OPs vary considerably, the above physical interpretation of the OPs hold, i.e., even after introducing dynamical reference configurations.

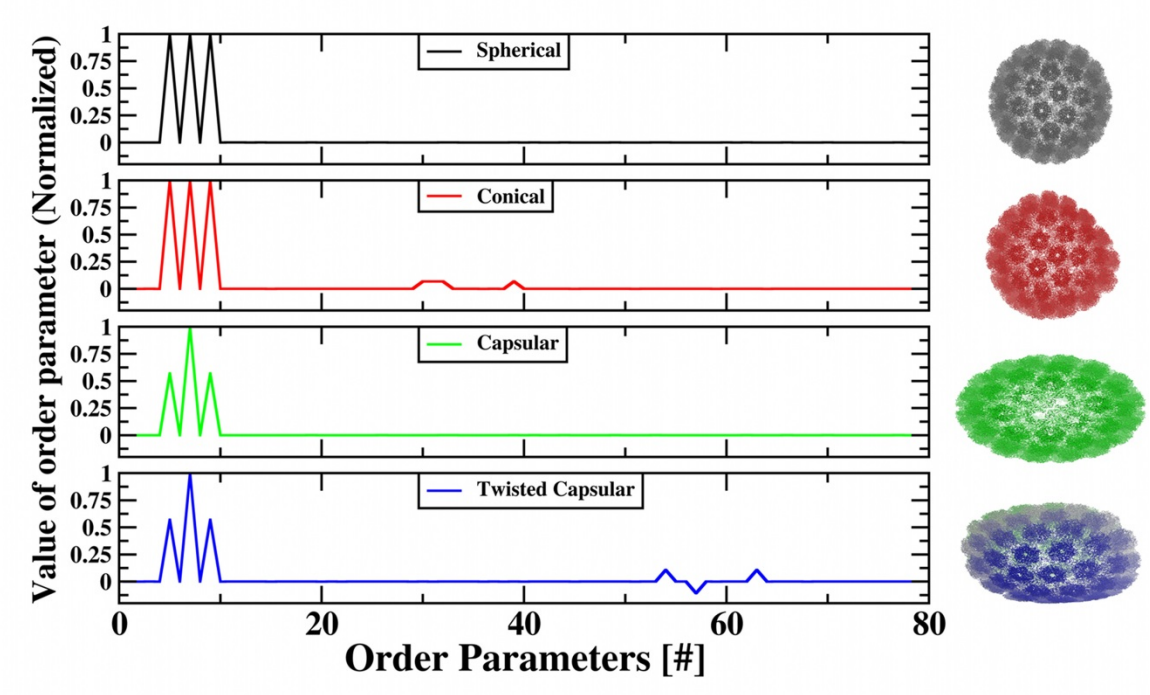

Fig. SI1 Normalized amplitude versus OP index $\underline{k}$. Space warping OPs with specified indices deform a T=7 capsid into conical, capsular, and twisted capsular forms. Cartesian components of only 3^3 OPs are chosen for this analysis, as they are sufficient to enable these transformations.

SI2. Ensemble Generation and Thermal Averaging

While several coarse-grained modeling approaches account for large-scale processes, important all-atom features of an assembly can be lost [7-14]. However, processes like the interaction of an antibody with a viral capsid can depend sensitively on atomic structure. To capture such details, in DMS, an ensemble of all-atom configurations consistent with the instantaneous OPs description is constructed. First, the state of scaled variables implying subsystem position (e.g., CM), shape and orientation are obtained such that they are consistent with the overall assembly architecture as provided by the set of global OPs (II.4). Then, an ensemble of all-atom configurations consistent with the subsystem CMs is generated. However, given only the location of subsystem CMs, this ensemble may contain many physically irrelevant structures that contribute little to the Boltzmann distribution. To address such issues, the number of intermediate scale variables is increased to include ones that account for the shape and orientation of subsystems, rather than just those that describe the position of their CM. With this, we introduce a set of variable $\bar{\varphi}_k^S$, where $\bar{\varphi}_0^S \equiv \vec{R}^S$ implies subsystem CMs and those with $k = \{100, 010, 001\}$ characterizes overall subsystem extension-contraction-rotation. In analogy to (II.11), these variables are used to construct $\vec{\boldsymbol{\Phi}}_k$ via

$$\vec{\boldsymbol{\Phi}}_k = \frac{1}{\mu_k} \sum_{S=1}^{N^{sys}} M^S U_k^S \left(\underline{\varphi}^S \right) \bar{\varphi}_k^S \,. \qquad \textbf{(S2.1)}$$

Now, consider an extended set $\underline{\varphi}_{ex}^S$ of subsystem-centered variables that include $\bar{\varphi}_k^S$ for k in the list of scaled variables that compose $\vec{\boldsymbol{\Phi}}_k$ (S2.1), plus additional variables $\bar{\varphi}_{kres}^S$ for *kres* not in the list of OP indices. As in (II.4), we write the position of atom *j* in subsystem *S* as

$$\vec{r}_j^{\,S} = \sum_k^{OP} \vec{\varphi}_k^S U_{kj}^S + \sum_{kres}^{res} \vec{\varphi}_{kres}^S U_{kj,res}^S \quad , \qquad \textbf{(S2.2)}$$

where $U_{kj}^S = U_k(\vec{r}_j^{\,S})$ and $U_{kj,res}^S = U_{kres}(\vec{r}_j^{\,S})$. This equation maps $\underline{\varphi}_{ex}^S$ onto the all-atom configuration variables $\underline{r}^S$. The mapping is one-to-one when the total number of $\vec{\varphi}_k^S$ and $\vec{\varphi}_{kres}^S$ equals the number of atoms in the subsystem *S,* n^S. With this, (S2.2) provides a way to generate an ensemble of atomic configurations consistent with a given value of $\vec{\varphi}_k^S$ (and hence global OPs $\vec{\Phi}_k$). For a set of fixed $\vec{\Phi}_k$, these configurations are achieved by randomly varying $\vec{\varphi}_{kres}^S$. For example, consider the evolution of $\vec{\Phi}_k$ constructed from $\vec{\varphi}_k^S$ with $k = \{000,100,010,001\}$; $S = 1,...,N^{sys}$. Ensembles of atomistic configurations consistent with the overall assembly structure defined via the values of $\underline{\Phi}$, and subassembly architecture provided by the lower-order $\underline{\varphi}^S$ are generated via changing those $\vec{\varphi}_k^S$ for which $\underline{k} \neq \{000,100,010,001\}$. By definition, such subsystem-centered variables evolve on a much shorter timescale relative to that of the global OPs [29]. Consequently, the system visits states for which the overall structure is conserved, yet the detailed atomistic configuration varies dramatically. This procedure accounts for small-scale incoherent displacement of each atom in addition to coherent deformations generated by the hierarchical OPs. Short MD runs are performed starting with configurations from this ensemble to arrive at an enriched ensemble that is consistent with a given set of global ($\underline{\Phi}$) and subsystem-centered variables.

The ensemble of all-atom structures using above procedure is employed to compute factors (thermal average forces $\vec{f}_k$ and diffusion factors $\vec{\vec{D}}_{kk'}$) that mediate the $\vec{\Psi}_k$ Langevin dynamics. The thermal average forces are derived in a manner similar to that derived in

Appendix C of Ref. [29]. This implies, $\vec{f}_k^{\Phi} = -\frac{\partial F}{\partial \vec{\Phi}_k} = \left\langle \vec{f}_k^{m} \right\rangle$, where $\vec{f}_k^{m} = \sum_S U_k^S \vec{F}_k^S$ is the global OP force, $\vec{F}_k^S = \sum_{i=1}^{N} \Theta_i^S U_{ki}^S \vec{F}_i^S$ is the subsystem-centered OP force and $\vec{F}_i^S$ is the force on the *i*-th atom in subsystem *S*. Similarly, $\vec{f}_i^{R} = -\frac{\partial F}{\partial \vec{R}^{S(i)}} = \left\langle M^S \sum_{i=1}^{N} \frac{\Theta_i^S \vec{F}_i^S}{m_i} \right\rangle$. The $\vec{f}_k$ are efficiently computed via an ensemble/Monte Carlo integration method enabled by the nature of our OPs. The atomic forces $\vec{F}_i^S$ computed for each member of an OP-constrained ensemble of atomic configurations are used to calculate the subsystem-centered OP forces $\vec{F}_k^S$, and ultimately the hierarchical OP forces $\vec{f}_k^{m}$. Monte Carlo integration averaging of $\vec{f}_k^{m}$ and $\vec{F}_j^S$ over the ensemble is carried out to obtain the thermal average force $\vec{f}_k^{\Phi}$ and $\vec{f}_i^{R}$. Short MD runs (~1 ps) are performed on configurations from this ensemble to calculate the OP velocity correlation functions. An ensemble average over multiple such correlations is needed to construct the $\vec{\vec{D}}_{kk'}$ (III.19-21). However, using only the early part of a single MD correlation function (wherein the most statics are accumulated) was found to suffice.

As in Eq. (II.4) we write the position of atom *j* in subsystem *S* as

$$\vec{r}_j^S = \sum_k^{OP} \vec{\varphi}_k^S U_{kj}^S + \vec{\sigma}_j^S, \qquad \textbf{(S2.3)}$$

where $\vec{\sigma}_j^S$ denotes the residual displacement of atom *j* resulting from a finite truncation of the k sum. Together (S2.1) and (S2.3) imply,

$$\vec{\sigma}_j^S = \sum_{kres}^{res} \vec{\varphi}_{kres}^S U_{kj,res}^S. \qquad \textbf{(S2.4)}$$

Multiplying (S2.4) by $U^S_{k'j,res}$, summing over all *j*, and using the orthogonality conditions we get

$$\vec{\varphi}^S_{kres} = \frac{\sum_{j=1}^{n^S} m^S_j U^S_{kj,res} \vec{\sigma}^S_j}{\sum_{i=1}^{n^S} m^S_j \{U^S_{kj,res}\}^2}. \qquad \textbf{(S2.5)}$$

Evolution of the all-atom ensemble may reflect in a systematic growth in the magnitude of residuals ($\vec{\sigma}^S_j$) and is observed in the cases we have studied earlier [29]. Major increase in residuals over time indicates the emergence of new intra-subsystem modes that are not captured by the initial set of OPs. Appearance of these modes, in turn, affects inter-subsystem or overall assembly dynamics. To account for such modes, OPs, $\vec{\varphi}^S_{kres}$, that were not included in the initial set of subsystem variables are constructed form the growing residuals via (S2.5), and added to the existing $\underline{\varphi}^S$ for the S^{th} subsystem. If the additional OPs are chosen properly then the residuals computed after using them will be negligible. Then the augmented $\underline{\varphi}^S$ is used to reconstruct a more extensive set of $\vec{\Phi}_k$ (S2.1). Thus, (S2.5) provides a way to discover the number of OPs that is both necessary and sufficient to describe the slow behavior of the system.

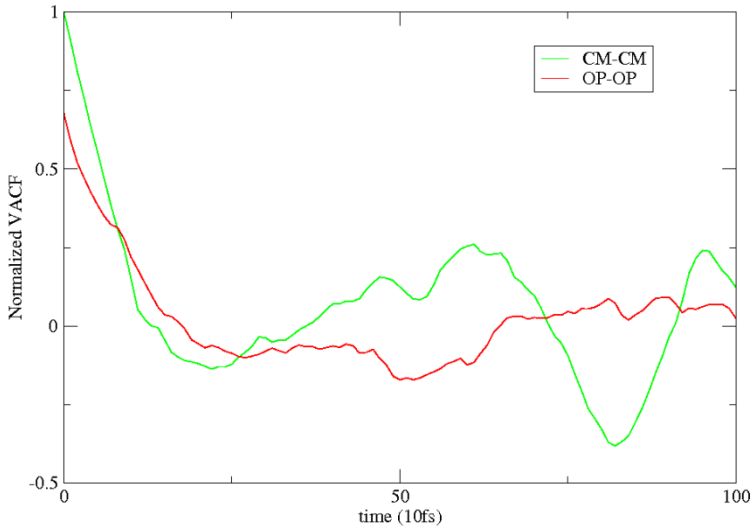

(a)

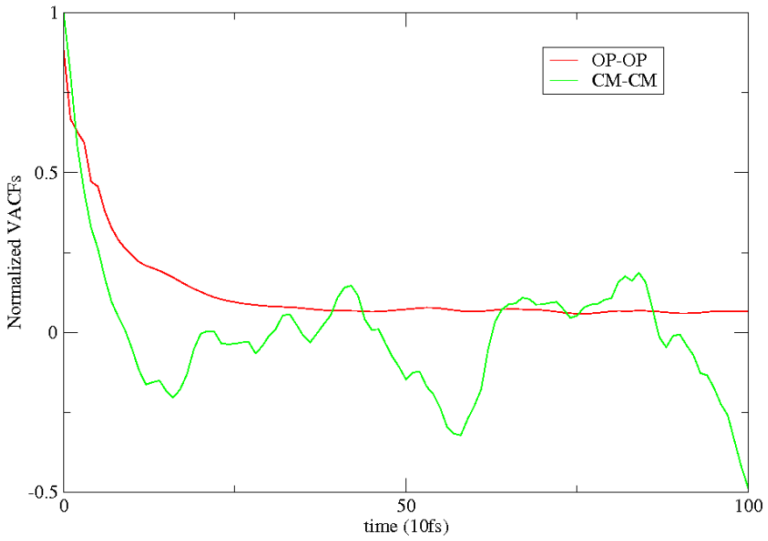

(b)

Fig. SI2 Normalized velocity autocorrelation functions (VACFs) showing **(a)** for the assembly the subsystem CM VACF decays much faster than that for a typical OP; however, the greater velocity marginally makes up for the loss in correlation so that diffusion coefficient of the CM is comparable to that of the lower-order ones. **(b)** Like in (a), for the free RNA, the CM VACF decays much faster than that for a typical OP. Since the correlation times associated with local motion is lesser than those for more global ones, the associated diffusion coefficients are lesser.

SI3. Diffusion Coefficient Comparison

The magnitude of diffusion coefficients depends on the velocity of the associated coarse-grained variables (e.g., OPs or CMs) and relaxation time of their correlation functions (III.19-22). Also, it is shown earlier that higher-order OPs describe more local motion than lower-order ones [19, 29-30]. Since the correlation times associated with local motions are lesser than those for more global ones, the associated diffusion coefficients are lesser (Fig. SI2). Consequently, for the RNA expansion, diffusion coefficients characterizing higher-order variables, which imply local motions, are less than those for lower-order ones that probe global motions. However, for the assembly problem, the difference in velocity between the higher and lower-order OPs (global and local modes) is much higher than that for the RNA. This reflects that protein monomers are strongly yet non-covalently interacting and therefore move more freely than the covalently bonded RNA pentamers. Even though the decay time for higher-order OP correlation is small, the greater velocity marginally accounts for the loss in correlation (Fig. SI2). Hence, diffusion coefficients of the higher-order OPs are comparable to those of the lower-order ones. Furthermore, since OPs with higher k probe smaller regions in space, the behavior of higher-order OPs is strongly correlated to intermediate scale variables such as subsystem CMs. This suggests that the behavior of higher-order $\bar{\bar{D}}_{kk}^{\Phi\Phi}$ should be similar to those of $\bar{\bar{D}}_{ii}^{RR}$, as is the case for both examples (Figs. 4(d) and SI3).

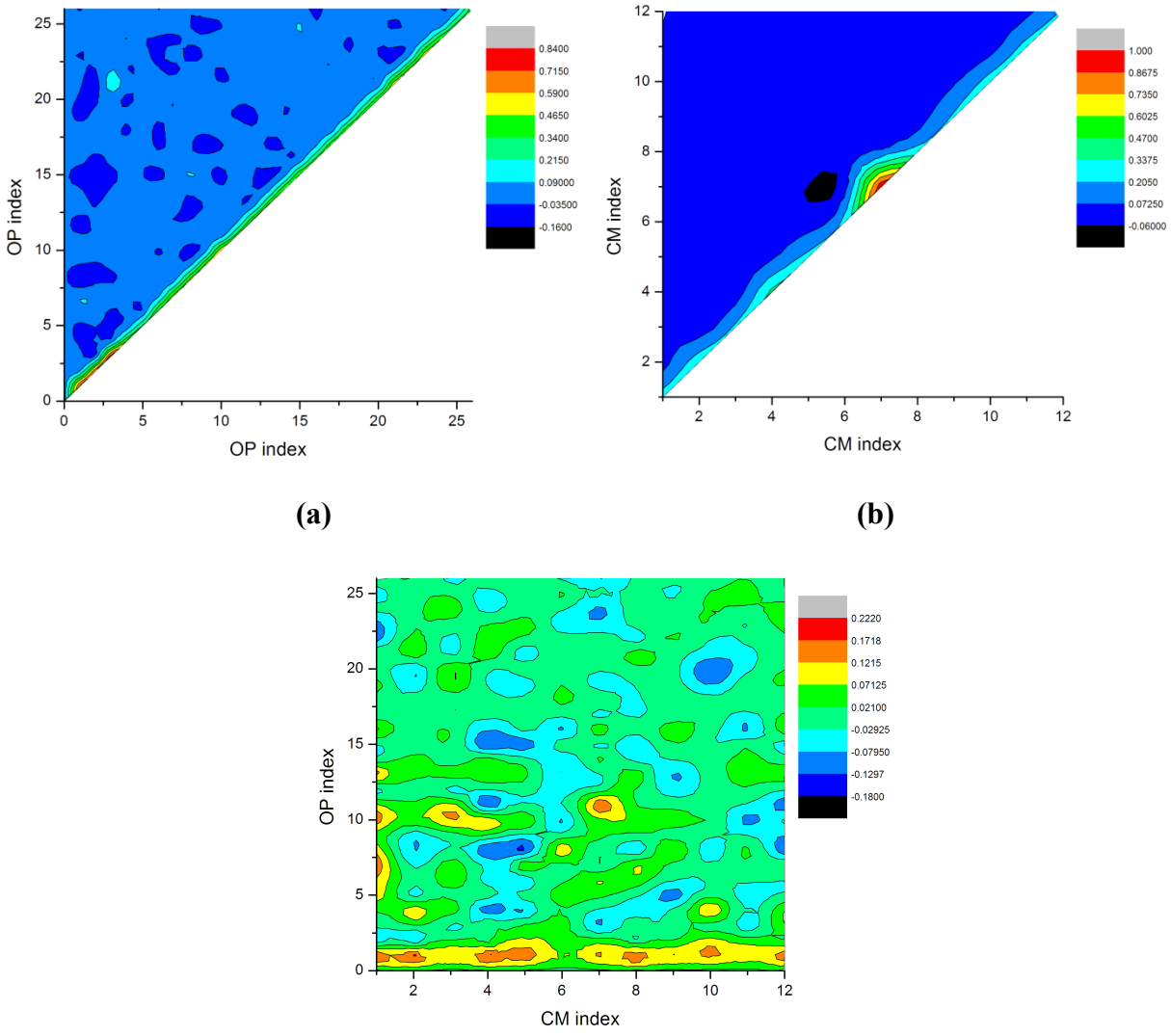

(a) **(b)**

(c)

Fig. SI3 Normalized diffusion matrices $\bar{\bar{D}}^{\Phi\Phi}_{kk'}$, $\bar{\bar{D}}^{RR}_{ij}$ and $\bar{\bar{D}}^{\Phi R}_{ik}$ with $k_1 + k_2 + k_3 \le 6$ (implying 3^3 OPs) and $S = 1,...,12$ showing $\bar{\bar{D}}^{\Phi\Phi}_{kk} >> \bar{\bar{D}}^{RR}_{ii} > \bar{\bar{D}}^{\Phi R}_{ik}$ for the expansion of free RNA aqueous solution.

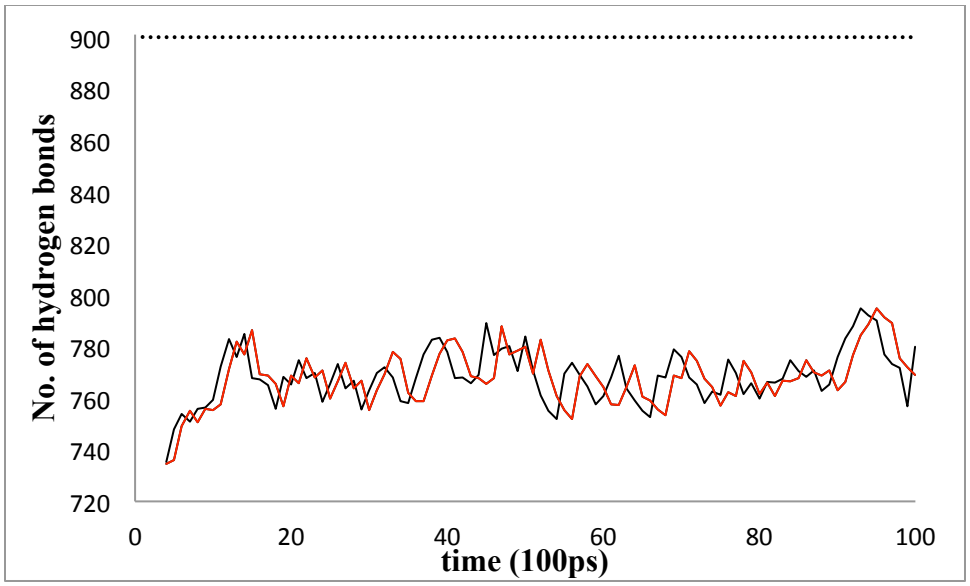

Fig. SI4 Number of inter-nucleic hydrogen bonds (MD: black, multiscale: red) gradually increases with time indicating the viral RNA gains more secondary structure as the monomers assemble around it. Also shown is the average number of hydrogen bonds present in the RNA in its capsid bound state (black dotted) as observed from previous simulations [9, 30]. Thus, the final RNA structure after 10ns (Fig. 9 (inset)) would require the involvement of ~20% more hydrogen bonds during subsequent assembly steps to resurrect its experimentally observed encapsidated state (Fig. 2(c)).